PHYSICAL REVIEW B **95**, 020103(R) (2017)

Pressure-stabilized hafnium nitrides and their properties

Jin Zhang,[1,*] Artem R. Oganov,[1,2,3,4,†] Xinfeng Li,[5] and Haiyang Niu[1]

[1]*Department of Geosciences, Center for Materials by Design, and Institute for Advanced Computational Science, State University of New York, Stony Brook, New York 11794-2100, USA*

[2]*Skolkovo Institute of Science and Technology, Skolkovo Innovation Center, 5 Nobel Street, Moscow 143026, Russia*

[3]*International Center for Materials Discovery, School of Materials Science and Engineering, Northwestern Polytechnical University, Xi'an, Shaanxi 710072, People's Republic of China*

[4]*Moscow Institute of Physics and Technology, Dolgoprudny, Moscow Region 141700, Russia*

[5]*State Key Laboratory for Mechanical Behavior of Materials, School of Materials Science and Engineering, Xi'an Jiaotong University, Xian 710049, People's Republic of China*

(Received 15 June 2016; published 18 January 2017)

We report hafnium nitrides under pressure using first-principles evolutionary calculations. Metallic $P6_3/mmc$-HfN (calculated Vickers hardness 23.8 GPa) is found to be more energetically favorable than NaCl-type HfN at zero and high pressure. Moreover, NaCl-type HfN actually undergoes a phase transition to $P6_3/mmc$-HfN below 670 K at ambient pressure. HfN_{10}, which simultaneously has infinite armchairlike polymeric N chains and N_2 molecules in its crystal structure, is discovered to be stable at moderate pressure above 23 GPa and can be preserved as a metastable phase at ambient pressure. At ambient conditions (298 K, 0 GPa), the gravimetric energy densities and the volumetric energy densities of HfN_{10} are 2.8 kJ/g and 14.1 kJ/cm^3, respectively.

DOI: 10.1103/PhysRevB.95.020103

Nitrides of group IVB elements (Ti, Zr, Hf), which are widely used in industry, exhibit an attractive combination of various physical and chemical features. Among them, hafnium nitrides (HfN_x) display high melting points (HfN: 3330 °C [1]), high incompressibility (HfN: $B_0 = 260$–306 GPa [2]; Hf_3N_4: $B_0 = 227$–260 GPa [3,4]), oxidation resistance at high temperatures [5], and superconductivity (HfN: $T_c = 8.8$ K) [6], and have been widely exploited by experiments [7–10] and calculations [8–11] in recent years.

Three decades ago, Rudy [12] and Lengauer [13] observed and studied ϵ-Hf_3N_2 ($R\bar{3}m$) and ζ-Hf_4N_3 ($R\bar{3}m$) which were unstable above ∼2000 and ∼2300 °C, respectively. Compared to hafnium subnitrides, researchers put more efforts into studying the structures and properties of HfN and Hf_3N_4. Experimental efforts [14] succeeded in growing single crystals of HfN by the zone-annealing technique and confirmed that metallic HfN crystallized in the rock-salt structure ($B1$) with a golden color. Theoretical investigations further indicated that NaCl ($B1$) type HfN will transform into CsCl ($B2$) type at a very high pressure (304 GPa [15] and 246 GPa [8]).

In 1991, a transparent Hf_3N_4 thin film was prepared by chemical vapor deposition (CVD) [16], though at that time researchers were not certain about its exact crystal structure. Now, thin films of Hf_3N_4 can also be deposited by atomic layer deposition (ALD) [17,18]. Compared with the Hf_3N_4 thin film, bulk Hf_3N_4 is more difficult to prepare because of its high melting point. The transparent semiconducting or insulating bulk Th_3P_4-type Hf_3N_4($I\bar{4}3d$), recoverable to ambient pressure, was synthesized by Zerr *et al.* [4] in laser-heated diamond anvil cells (LH-DACs) at pressures up to 18 GPa and temperatures up to 3000 K. Subsequently, Salamat [7] crystallized a tetragonal $I4/m$-Hf_3N_4 polymorph at 12 GPa and 1500 K and a high-pressure orthorhombic $Pnma$-Hf_3N_4 polymorph at 19 GPa and 2000 K using LH-DACs. Meanwhile, first-principles calculations [11,15,19] showed that orthorhombic $Pnma$-Hf_3N_4 was the most stable structure at ambient pressure and Th_3P_4-type Hf_3N_4 was predicted to be stable above 9 GPa at 0 K [19].

Another motivation to study nitrogen compounds under pressure is that at impractically high pressures (>110 GPa [20]) polymeric nitrogen is formed—the archetypal high-energy-density material (HEDM). Numerous theoretical [21–25] and experimental [26–28] studies tried to predict and synthesize polymeric forms of nitrogen or nitrogen-bearing compounds that can exist at ambient conditions. Virtually no work explored transition metal nitrides as a possibility to achieve polymerization of nitrogen at milder pressures.

Here, we report a theoretical pressure-composition phase diagram for a Hf-N system, and also prove the existence of $P6_3/mmc$-HfN and found HfN_{10} with polymeric nitrogen chains, as will be discussed below. The stable phases in the Hf-N system at pressures up to 60 GPa are searched by using the first-principles evolutionary algorithm (EA) as implemented in the USPEX code [29–31] combined with *ab initio* structure relaxations using density functional theory (DFT) with the Perdew-Burke-Ernzerhof generalized gradient approximation (PBE-GGA) functional [32], as implemented in the VASP package [33]. The electron-ion interaction was described by projector-augmented wave (PAW) potentials [34], with $5p^6 6s^2 5d^2$ and $2s^2 2p^3$ shells treated as the valence for Hf and N, respectively. Subsequent calculations of the phase transition and properties rely on well-converged structures (a total energy convergence less than 1 meV/atom) with respect to the plane-wave energy cutoff (600 eV) and Γ-centered uniform k meshes ($2\pi \times 0.06$ Å^{-1}). For comparison and verification, a local density approximation (LDA) is also used in calculating the free energy of some structures. Unless indicated otherwise, the calculations were done using the GGA. Phonon dispersions were calculated using the finite-displacement method in PHONOPY code [35]. The

*jin.zhang.1@stonybrook.edu
†artem.oganov@stonybrook.edu

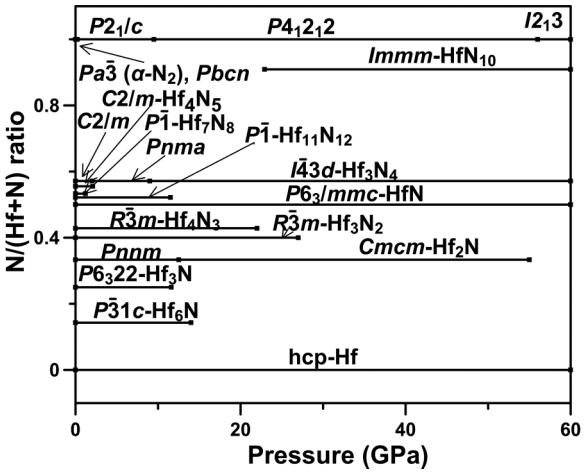

FIG. 1. Pressure-composition phase diagram of the Hf-N system.

Voight-Reuss-Hill (VRH) approximation was adopted for estimating the polycrystalline bulk modulus (B) and shear modulus (G).

Based on the global minimum of the free energy, we derived the pressure-composition phase diagram of the Hf-N system, as depicted in Fig. 1. Ten structures, including $P\bar{3}1c$-Hf_6N, $P6_322$-Hf_3N, $Pnnm$-Hf_2N, $R\bar{3}m$-Hf_3N_2, $R\bar{3}m$-Hf_4N_3, $P6_3/mmc$-HfN, $P\bar{1}$-$Hf_{11}N_{12}$, $P\bar{1}$-Hf_7N_8, $C2/m$-Hf_4N_5, and $C2/m$-Hf_3N_4, are stable at zero pressure (see Supplemental Material Table S1 [36] for the calculated structural parameters). All the other high-pressure Hf-N compounds can be decompressed to ambient conditions as metastable phases since they are mechanically and dynamically stable at 0 GPa (see Supplemental Material Fig. S2 [36]). The stoichiometries Hf_6N and Hf_3N were not reported by experiments, while previous Monte Carlo simulations [37] predicted the existence of Hf_6N and Hf_3N, and also indicated that the ground state of Hf_6N was $P\bar{3}1c$-Hf_6N while the Hf_3N belonged to $R\bar{3}c$ or $P6_322$-Hf_3N. Our calculations, with or without considering the zero point energy (ZPE), both showed that $P\bar{3}1c$-Hf_6N is the most stable (note the free energy $P\bar{3}1c$-Hf_6N is slightly lower than that of $R\bar{3}$-Hf_6N), and also indicated $P6_322$-Hf_3N is more stable that $R\bar{3}c$-Hf_3N at low pressures. Unlike $P4_2/mnm$-Ti_2N (the stable phase for Ti_2N at 0 GPa), Hf_2N is more energetically favorable in an orthorhombic phase (space group $Pnnm$); this $Pnnm$-Hf_2N transforms to $Cmcm$-Hf_2N at 12.5 GPa and $Cmcm$-Hf_2N continues to be stable up to 55 GPa [Fig. 2(a)]. Experimental high-temperature structures $R\bar{3}m$-Hf_3N_2 and $R\bar{3}m$-Hf_4N_3 [12,13] (experimental compositions $Hf_3N_{1.69}$ and $Hf_4N_{2.56}$) are also found to be stable at lower pressures and will decompose at 27 and 22 GPa, respectively.

Interesting and beyond expectation, it turns out the ground state of HfN should be metallic $P6_3/mmc$-HfN instead of NaCl-type ($B1$) HfN, which has been numerously reported in the literature [8,11,19]. Note that the structure of our $P6_3/mmc$-HfN with eight atoms in its unit cell is different from the NiAs-type HfN, which also has a space group $P6_3/mmc$, with four atoms in its unit cell. The ground state $B1$ is 0.0187 eV/atom (without ZPE) or 0.0138 eV/atom (with ZPE), which is higher in energy than $P6_3/mmc$-HfN. In order

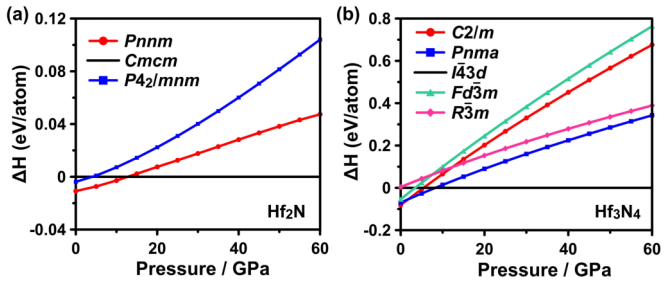

FIG. 2. Enthalpy-pressure diagrams of Hf_2N and Hf_3N_4. $Cmcm$-Hf_2N and $I\bar{4}3d$-Hf_3N_4 are taken as a reference for Hf_2N and Hf_3N_4, respectively. $Fd\bar{3}m$-Hf_3N_4 belongs to the spinel type.

to verify our calculations, as well as to compare with previous studies, the relative enthalpies of $P6_3/mmc$-HfN and $B1$-HfN (without ZPE) are plotted up to 300 GPa in Figs. 3(a) and 3(c). $P6_3/mmc$-HfN is more stable than $B1$-HfN at all pressures up to 300 GPa and the transition between $P6_3/mmc$-HfN and CsCl-type ($B2$) HfN appears at 287 GPa (270 GPa in LDA). The transformation pressure from $B1$ to $B2$ is 275 GPa (258 GPa in LDA), which is comparable to the previous GGA result of 301 GPa [15].

$P6_3/mmc$-HfN actually consists of a double close packed hexagonal (dhcp) lattice of Hf atoms, with nitrogen atoms filling all octahedral voids, as seen in Fig. 4(a). The Hf-N

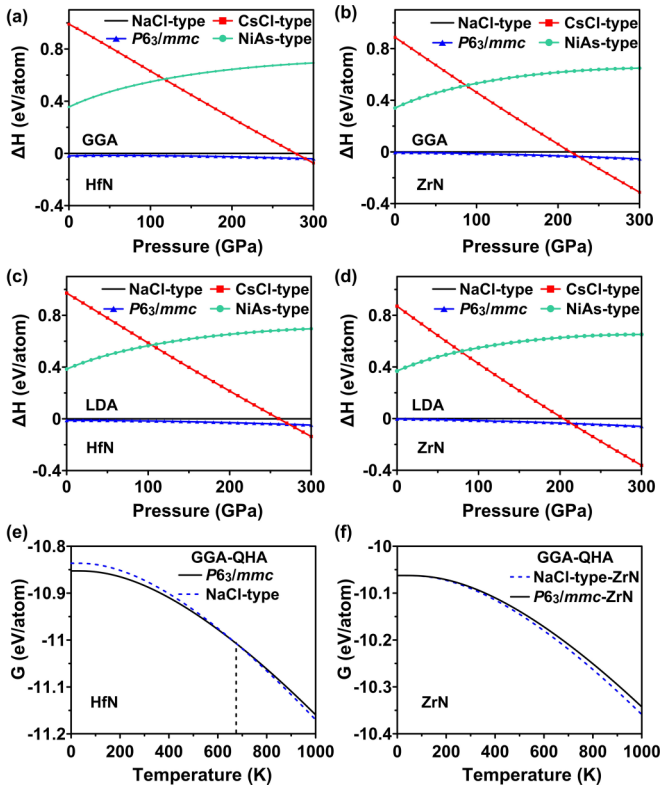

FIG. 3. Enthalpy-pressure diagrams of HfN and ZrN in (a), (b) GGA and (c), (d) LDA, respectively (relative to the NaCl-type HfN and NaCl-type ZrN), and (e), (f) free enthalpy as a function of temperature of $P6_3/mmc$ and NaCl-type structures for HfN and ZrN obtained by the quasiharmonic approximation (QHA) method and the GGA.

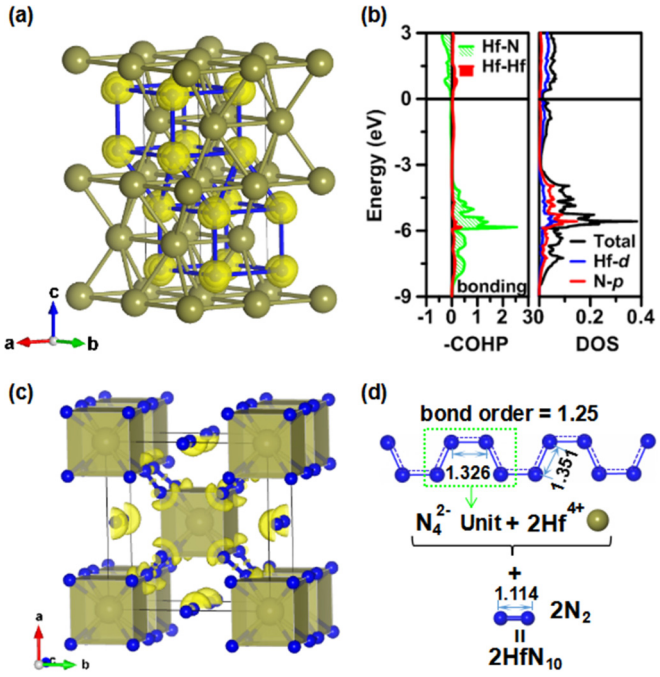

FIG. 4. ELF isosurface (ELF = 0.85) of (a) $P6_3/mmc$-HfN and (c) $Immm$-HfN_{10} at 0 GPa, (b) density of states and COHP for $P6_3/mmc$-HfN, and (d) the composition illustration of $Immm$-HfN_{10} (the bond length is in Å). Hf-centered polyhedra are dark yellow; part of the infinite N chain and N≡N bonds are also displayed in (d). Large gray spheres, Hf atoms; small blue spheres, N atoms.

covalent bond can be revealed by the hybridization between the Hf-d and N-p orbitals in Fig. 4(b); the Hf-Hf and Hf-N bonding characters can be reflected by calculating the crystal orbital Hamilton population (COHP) [38] using the tight-binding linear muffin-tin orbital atomic sphere approximation (TB-LMTO-ASA) program [39]. Based on the quasiharmonic approximation (QHA), $P6_3/mmc$-HfN will transform into $B1$-HfN at 670 K (397 °C), as shown in Fig. 3(e).

Ti and Zr are in the same group with Hf, and especially Zr has a strong chemical similarity with Hf. The existence of hexagonal HfN naturally leads to the question as to whether similar structures can exist for TiN and ZrN. Thus we computed the enthalpy-pressure diagrams of ZrN and TiN in the GGA and LDA. For the enthalpy-pressure diagram of TiN (without ZPE, see Supplemental Material Fig. S3 [36]), the ground-state energy of $P6_3/mmc$-TiN is 0.0344 eV/atom higher than that of $B1$-TiN, thus $B1$-TiN is still the most stable structure at 0 GPa. The case of ZrN is tricky. As shown in Table I, $P6_3/mmc$-ZrN is 0.0052 eV/atom (without ZPE) higher than $B1$-ZrN in free energy while $B1$-ZrN is 0.0006 eV/atom energetically higher than $P6_3/mmc$-ZrN with ZPE. This is not surprising, because the ZPEs for $P6_3/mmc$-HfN and $B1$-HfN are 0.0625 and 0.0572 eV/atom, respectively, and for $P6_3/mmc$-ZrN and $B1$-ZrN they are 0.0642 and 0.0584 eV/atom, respectively, and along with the energy difference (0.0052 eV/atom, without ZPE) between $P6_3/mmc$-ZrN and $B1$-ZrN being too small compared with the energy difference (0.0186 eV/atom, without ZPE) between $P6_3/mmc$-HfN and B1-HfN; so when the ZPE is considered, $B1$-ZrN becomes more stable than $P6_3/mmc$-ZrN.

TABLE I. Calculated lattice parameters a and c, bulk modulus B_0, its pressure derivation B_0' (calculated parameters were fit to a third-order Birch-Murnaghan equation of state), equilibrium volume V_0, free energy without ZPE E, and free energy with ZPE E_0.

	HfN		ZrN	
Parameter	$P6_3/mmc$	$B1$	$P6_3/mmc$	$B1$
a (Å)	3.1791	4.5373	3.2349	4.6169
c (Å)	10.6976		10.8626	
B_0 (GPa)	265.37	270.16	245.04	247.91
B_0'	4.255	4.289	4.239	4.282
V_0 (Å^3)	93.63	93.41	98.45	98.41
E (eV/atom)	–10.9126	–10.8940	–10.1259	–10.1207
E_0 (eV/atom)	–10.8501	–10.8368	–10.0617	–10.0623

The computed Gibbs free energies [Fig. 3(f)] show that we cannot expect that $P6_3/mmc$-ZrN will, as $P6_3/mmc$-HfN, become stable at ambient conditions. However, with increasing pressure, $P6_3/mmc$-ZrN becomes more stable than $B1$-ZrN [see Figs. 3(b) and 3(d)]. The transition pressure from $P6_3/mmc$-ZrN to $B2$-ZrN is 221 GPa (212 in LDA), and the value of the metastable transition pressure from $B1$-ZrN to $B2$-ZrN is 211 GPa (201 in LDA), which is in accordance with previous GGA calculations: 205 GPa from Hao's work [40] and 208 GPa from Kroll's work [15].

Based on our calculations, we can theoretically conclude that for $P6_3/mmc$-TiN, $P6_3/mmc$-ZrN, and $P6_3/mmc$-HfN, only $P6_3/mmc$-HfN is stable at ambient conditions. However, why is $P6_3/mmc$-HfN not experimentally found? Seen from the Hf-N equilibrium diagram, NaCl-type HfN appears above 500 °C [41]. In fact, experiments which tried to synthesize HfN crystal, HfN films, or HfN powder always operated at temperatures above 400 °C. A single crystal of HfN was grown by the zone-annealing technique with a temperature of approximately 2500 °C [14]. Fabricating HfN film by chemical vapor deposition (CVD) generally needs to take place at high temperatures above 1000 °C [16]; physical vapor deposition (PVD)-reactive sputtering is also used to synthesize HfN at 450 °C [42]. At room temperature, hafnium nitride films can be formed by ion beam synthesis [43], but these hafnium nitride films are a mixture, Hf_3N_2, Hf_4N_3, and HfN.

Three metallic Hf-vacancy nitrides, including $P\bar{1}$-$Hf_{11}N_{12}$, $P\bar{1}$-Hf_7N_8, and $C2/m$-Hf_4N_5, are stable at 0 GPa, consistent with the stoichiometries proposed by experiments of Hf vacancies contained in HfN_x film ($x > 1$) [9,10]. The ground-state phase we find for Hf_3N_4 is not the orthorhombic Zr_3N_4 type ($Pnma$) which was proposed [15,19] earlier. Instead, a monoclinic $C2/m$-Hf_3N_4 is more energetically favorable than $Pnma$-Hf_3N_4. With increasing pressure, two transitions occur in Hf_3N_4: $C2/m$-Hf_3N_4 → $Pnma$-Hf_3N_4 at 2 GPa and $Pnma$-Hf_3N_4 → Th_3P_4-type Hf_3N_4 at 9 GPa [Fig. 2(b)].

Another interesting metallic structure, $Immm$-HfN_{10} with every Hf atom coordinated by eight N atoms, is stable at pressures above 23 GPa. This structure simultaneously contains encapsulated N_2 molecules with triple N≡N bonds (the bond length is 1.114 Å) and an infinite polymeric N chain. Electrons are delocalized over the whole infinite polymeric N chain. Each N-N bond in the infinite polymeric

TABLE II. Pressure range (PR) of the stability of Hf-N compounds and their calculated zero-pressure elastic properties (polycrystalline bulk modulus B, shear modulus G, Young's modulus E, Poisson's ratio υ, and Vickers hardness). G/B and υ are dimensionless; PR, B, G, E and H_v are in GPa.

Compound	PR	B_H	G_H	E	G/B	υ	H_v
$P\bar{3}1c$-Hf_6N	0–14	128.4	68.8	175.1	0.54	0.273	8.4
$P6_322$-Hf_3N	0–11.6	154.8	79.6	204.0	0.51	0.281	8.9
$Pnnm$-Hf_2N	0–12.5	189.4	113.3	283.4	0.60	0.251	14.4
$Cmcm$-Hf_2N	12.5–55	170.1	106.0	263.2	0.62	0.242	14.6
$R\bar{3}m$-Hf_3N_2	0–27	212.5	134.5	333.2	0.63	0.238	17.6
$R\bar{3}m$-Hf_4N_3	0–22	223.0	131.1	328.8	0.59	0.254	15.6
$P6_3/mmc$-HfN	0–60	264.1	180.6	441.3	0.68	0.221	23.8
NiAs-type HfN		242.5	128.8	328.3	0.53	0.274	13.4
NaCl-type HfN		267.9	163.0	406.5	0.61	0.247	19.0
$P\bar{1}$-$Hf_{11}N_{12}$	0–11.5	259.4	176.2	431.0	0.68	0.223	23.2
$P\bar{1}$-Hf_7N_8	0–1.2	253.0	173.4	423.5	0.69	0.221	23.2
$C2/m$-Hf_4N_5	0–2.1	235.5	162.2	395.7	0.69	0.226	22.4
$C2/m$-Hf_3N_4	0–2	225.5	159.0	386.1	0.71	0.214	22.8
$Pnma$-Hf_3N_4	2–9	208.4	100.5	259.8	0.48	0.292	9.6
$I\bar{4}3d$-Hf_3N_4	9–60	216.0	124.5	313.4	0.58	0.258	14.7
$Immm$-HfN_{10}	23–60	150.4	94.8	235.0	0.63	0.240	13.7

N chain is an intermediate bond between single and double bonds, as shown in Fig. 4(d). In addition, we find that $Immm$-ZrN_{10} and $Immm$-TiN_{10} can also be metastable structures (dynamically and mechanically stable) at ambient pressure. The gravimetric energy density for $Immm$-TiN_{10} is 5.2 kJ/g at ambient conditions (298 K, 0 GPa), higher than that for the well-known explosive material 2,4,6-trinitrotoluene (TNT) (4.3 kJ/g) and mildly lower than another powerful explosive octahydro-1,3,5,7-tetranitro-1,3,5,7-tetrazocine (HMX) (5.7 kJ/g) [44]. The gravimetric energy densities for $Immm$-HfN_{10} and $Immm$-ZrN_{10} are 2.8 and 3.6 kJ/g at ambient conditions, respectively, and the volumetric energy densities of HfN_{10}, ZrN_{10}, and TiN_{10} are correspondingly 14.1, 12.9, and 16.4 kJ/cm^3 (see Supplemental Material [36] for detailed energy density calculations), which are higher than TNT (7.2–8.0 kJ/cm^3), 1,3,5-trinitroperhydro-1,3,5-triazine (RDX) (10.1 kJ/cm^3), and pentaerythritol tetranitrate (PETN) (10.6 kJ/cm^3) [45,46].

The elastic moduli of all the Hf-N compounds are calculated according to the elastic constant tensors and theoretical hardnesses can be further predicted based on the Chen-Niu's empirical correlation [47] as listed in Table II. $P6_3/mmc$-HfN exhibits the highest shear modulus (180.6 GPa) and its calculated hardness is 23.8 GPa. It is worthwhile to note that Hf-vacancy containing structures, including $P\bar{1}$-$Hf_{11}N_{12}$, $P\bar{1}$-Hf_7N_8, $C2/m$-Hf_4N_5, and $C2/m$-Hf_3N_4, also show high hardnesses. The G/B ratio, proposed by Pugh [48], can be used to judge the brittleness and ductility of materials: $G/B > 0.57$ corresponds to brittle and $G/B < 0.57$ to ductile behavior. $C2/m$-Hf_3N_4 is the most brittle, while $Pnma$-Hf_3N_4 is the most ductile among the Hf-N compounds. Moreover, G/B can also represent the directionality of bonding in the material [49]. $P6_3/mmc$-HfN and $C2/m$-Hf_3N_4 have a strong covalent (directional) component of bonding which has a positive effect on their hardnesses. Increasing the nitrogen content in subnitrides can improve their mechanical properties due to the formation of additional Hf-N bonds. For nitrogen-rich compounds, the effect of nitrogen content on mechanical properties is minor and the atomic configuration becomes the main factor determining the mechanical properties.

In summary, we predicted the pressure-composition phase diagram of the Hf-N system. Several intriguing phases and stoichiometries are found. Metallic $P6_3/mmc$-HfN with the highest hardness (23.8 GPa) among Hf-N compounds should be the ground state for HfN and will transform into NaCl-HfN at 670 K at ambient pressure. Semiconducting $C2/m$-Hf_3N_4 has a lower energy than the previously proposed $Pnma$-Hf_3N_4 at 0 GPa. The calculated hardnesses of all the predicted high-pressure Hf-N phases range from 8.4 to 23.8 GPa at 0 GPa. It is noteworthy that Hf vacancies do not degrade the mechanical properties of nitrides, e.g., both Hf_7N_8 and $Hf_{11}N_{12}$ exhibit good hardnesses. HfN_{10}, containing polymeric nitrogen chains, is predicted to become stable at pressures above 23 GPa. Meanwhile, it is a potential high-energy-density material because of its good gravimetric (2.8 kJ/g) and volumetric energy densities (14.1 kJ/cm^3). This work provides an important guide for experiments to synthesize HfN_{10}, an analog of polymeric nitrogen, at moderate pressures, and HfN_{10} also has a possibility to be kept as a metastable phase at ambient pressure based on our analysis.

This work was supported by DARPA (No. W31P4Q1210008), the Foreign Talents Introduction, the Academic Exchange Program of China (No. B08040), and the top-S-100 project of MIPT. Calculations were carried out the Extreme Science and Engineering Discovery Environment (XSEDE), which is supported by National Science Foundation Grant No. ACI-1053575.

[1] M. Wittmer, J. Vac. Sci. Technol. A **3**, 1797 (1985).
[2] X.-J. Chen, V. V. Struzhkin, Z. Wu, M. Somayazulu, J. Qian, S. Kung, A. N. Christensen, Y. Zhao, R. E. Cohen, H.-k. Mao *et al.*, Proc. Natl. Acad. Sci. USA **102**, 3198 (2005).
[3] D. A. Dzivenko, A. Zerr, R. Boehler, and R. Riedel, Solid State Commun. **139**, 255 (2006).
[4] A. Zerr, G. Miehe, and R. Riedel, Nat. Mater. **2**, 185 (2003).
[5] M. M. Opeka, I. G. Talmy, E. J. Wuchina, J. A. Zaykoski, and S. J. Causey, J. Eur. Ceram. Soc. **19**, 2405 (1999).
[6] H. O. Pierson, *Handbook of Refractory Carbides and Nitrides: Properties, Characteristics, Processing and Apps* (William Andrew, Norwich, NY, 1996).
[7] A. Salamat, A. L. Hector, B. M. Gray, S. A. Kimber, P. Bouvier, and P. F. McMillan, J. Am. Chem. Soc. **135**, 9503 (2013).

[8] M. Chauhan and D. C. Gupta, Int. J. Refract. Hard Met. **42**, 77 (2014).
[9] C. Hu, Z. Gu, J. Wang, K. Zhang, X. Zhang, M. Li, S. Zhang, X. Fan, and W. Zheng, J. Phys. Chem. C **118**, 20511 (2014).
[10] Z. Gu, C. Hu, H. Huang, S. Zhang, X. Fan, X. Wang, and W. Zheng, Acta Mater. **90**, 59 (2015).
[11] H. Huang, X. Fan, C. Hu, D. J. Singh, Q. Jiang, and W. Zheng, J. Phys.: Condens. Matter **27**, 225501 (2015).
[12] E. Rudy, Metall. Mater. Trans. **1**, 1249 (1970).
[13] W. Lengauer, D. Rafaja, G. Zehetner, and P. Ettmayer, Acta Mater. **44**, 3331 (1996).
[14] A. N. Christensen, W. Kress, M. Miura, and N. Lehner, Phys. Rev. B **28**, 977 (1983).
[15] P. Kroll, J. Phys.: Condens. Matter **16**, S1235 (2004).
[16] R. Fix, R. G. Gordon, and D. M. Hoffman, Chem. Mater. **3**, 1138 (1991).
[17] K. Y. Ahn and L. Forbes, Atomic layer deposition of Hf_3N_4/HfO_2 films as gate dielectrics, U.S. Patent No. 7,498,247 (3 March 2009).
[18] J. S. Becker, E. Kim, and R. G. Gordon, Chem. Mater. **16**, 3497 (2004).
[19] P. Kroll, Phys. Rev. Lett. **90**, 125501 (2003).
[20] M. I. Eremets, R. J. Hemley, H.-k. Mao, and E. Gregoryanz, Nature (London) **411**, 170 (2001).
[21] W. D. Mattson, D. Sanchez-Portal, S. Chiesa, and R. M. Martin, Phys. Rev. Lett. **93**, 125501 (2004).
[22] F. Zahariev, A. Hu, J. Hooper, F. Zhang, and T. Woo, Phys. Rev. B **72**, 214108 (2005).
[23] Y. Yao, J. S. Tse, and K. Tanaka, Phys. Rev. B **77**, 052103 (2008).
[24] Y. Ma, A. R. Oganov, Z. Li, Y. Xie, and J. Kotakoski, Phys. Rev. Lett. **102**, 065501 (2009).
[25] H. Yu, D. Duan, F. Tian, H. Liu, D. Li, X. Huang, Y. Liu, B. Liu, and T. Cui, J. Phys. Chem. C **119**, 25268 (2015).
[26] M. I. Eremets, A. G. Gavriliuk, I. A. Trojan, D. A. Dzivenko, and R. Boehler, Nat. Mater. **3**, 558 (2004).
[27] I. Trojan, M. Eremets, S. Medvedev, A. Gavriliuk, and V. Prakapenka, Appl. Phys. Lett. **93**, 091907 (2008).
[28] D. Tomasino, M. Kim, J. Smith, and C.-S. Yoo, Phys. Rev. Lett. **113**, 205502 (2014).
[29] A. R. Oganov and C. W. Glass, J. Chem. Phys. **124**, 244704 (2006).
[30] A. O. Lyakhov, A. R. Oganov, H. T. Stokes, and Q. Zhu, Comput. Phys. Commun. **184**, 1172 (2013).
[31] A. R. Oganov, A. O. Lyakhov, and M. Valle, Acc. Chem. Res. **44**, 227 (2011).
[32] J. P. Perdew, K. Burke, and M. Ernzerhof, Phys. Rev. Lett. **77**, 3865 (1996).
[33] G. Kresse and J. Furthmüller, Phys. Rev. B **54**, 11169 (1996).
[34] P. E. Blöchl, Phys. Rev. B **50**, 17953 (1994).
[35] A. Togo, F. Oba, and I. Tanaka, Phys. Rev. B **78**, 134106 (2008).
[36] See Supplemental Material at http://link.aps.org/supplemental/10.1103/PhysRevB.95.020103 for the calculated structural parameters (Table S1); convexhull diagrams of Hf-N system at different pressures (Fig. S1); calculated phonon dispersion curves for Hf-N compounds at 0 GPa (Fig. S2); enthalpy-pressure diagrams of TiN (Fig. S3); band structures and density of states for hafnium nitrides at 0 GPa (Fig. S5) and detailed energy density calculations.
[37] A. V. Ruban, V. I. Baykov, B. Johansson, V. V. Dmitriev, and M. S. Blanter, Phys. Rev. B **82**, 134110 (2010).
[38] R. Dronskowski and P. E. Bloechl, J. Phys. Chem. **97**, 8617 (1993).
[39] G. Krier, O. Jepsen, A. Burkhardt, and O. K. Andersen, The TB-LMTO-ASA program, Stuttgart, Germany, 1995, http://www.mpi-stuttgart.mpg.de.
[40] A. Hao, T. Zhou, Y. Zhu, X. Zhang, and R. Liu, Mater. Chem. Phys. **129**, 99 (2011).
[41] H. Okamoto, J. Phase Equilib. **11**, 146 (1990).
[42] S. Shinkai and K. Sasaki, Jpn. J. Appl. Phys. **38**, 2097 (1999).
[43] A. Arranz, Surf. Sci. **563**, 1 (2004).
[44] B. Dobratz and P. Crawford, LLNL Handbook of Explosives, Lawrence Livermore National Laboratory, Technical Report No. UCRL-52997, 1985 (unpublished).
[45] D. W. Smith, S. T. Iacono, and S. S. Iyer, *Handbook of Fluoropolymer Science and Technology* (Wiley, Hoboken, NJ, 2014).
[46] K. S. Martirosyan, J. Mater. Chem. **21**, 9400 (2011).
[47] X.-Q. Chen, H. Niu, D. Li, and Y. Li, Intermetallics **19**, 1275 (2011).
[48] S. Pugh, Philos. Mag. **45**, 823 (1954).
[49] K. Tanaka, K. Okamoto, H. Inui, Y. Minonishi, M. Yamaguchi, and M. Koiwa, Philos. Mag. A **73**, 1475 (1996).